Raman Spectroscopy of Supported Metal Oxide Catalysts

Israel E. Wachs, Franklin D. Hardcastle, and Shirley S. Chan

Exxon Research and Engineering Company

The fundamental information that is currently being obtained from laser Raman characterization of supported metal oxide catalysts is reviewed. The Raman vibrational spectra reveal that the states of the supported metal oxides are very different from their bulk, unsupported oxide counterparts. The ability to discriminate between different states allows the determination of which parameters control the metal oxide phases present in supported metal oxides. For example, the structural transformations that occur at elevated temperatures in the supported metal oxide systems are readily monitored using Raman spectroscopy, and the important parameter controlling the metal oxide phases for many of these systems, such as WO_3/Al_2O_3, is the surface density of the surface metal oxide. In situ Raman spectroscopy studies provide additional information about the nature of the surface metal oxide and distinguish between metal oxides that are adsorbed on the alumina support surface and metal oxides that appear to be absorbed into the alumina support surface. Information about the structure of the surface metal oxide is also contained in the Raman vibrational spectrum, and the structures of surface rhenium oxide on alumina, ReO_4, and surface chromium oxide on alumina, CrO_4 and Cr_2O_7, are presented. Recent catalytic studies have shown that the surface metal oxides are responsible for the activity and selectivity of many supported metal oxide catalysts.

Supported metal oxides are formed when one metal oxide phase is dispersed on a second metal oxide substrate. Supported metal oxides are widely used as catalysts to accelerate chemical reactions and control reaction selectivity in the petroleum and chemical industries. Many of the petroleum and chemical processes use catalysts (1), and a significant portion of these catalysts is in the form of supported metal oxides (2,3). Catalysts also are used extensively to reduce automobile and industrial plant emissions (1). Most commercial catalysts contain alumina (Al_2O_3), silica (SiO_2), or titania (TiO_2) as the metal oxide substrate. When a metal oxide is dispersed on a second metal oxide substrate, the supported metal oxide phase can simultaneously possess several different chemical states. The multiple chemical states that can simultaneously be present in the supported metal oxide phase have acted as a source of confusion and have hampered progress in the understanding of supported metal oxide catalysts because of the lack of applicable characterization techniques that can discriminate between these different states. Conventional catalyst characterization techniques provide some general information about the supported metal oxide phase, but they are not adequate to discriminate between the different chemical states that are simultaneously present (4). In the past few years, however, characterization studies of supported metal oxides have shown that the different chemical states in the supported metal oxide phase can be discriminated with the use of laser Raman spectroscopy (5–65). This technique can discriminate between the different chemical states of the supported metal oxides because each state possesses a unique vibrational spectrum that is related to its structure. Therefore, Raman spectroscopy provides direct information about the structure of each state as well as a method to discriminate between the various states. To date, the supported metal oxides studied with Raman spectroscopy include molybdenum oxide (5–37), tungsten oxide (12–14, 20, 25, 31, 38–48), vanadium oxide (31, 49–59), rhenium oxide (60–62), chromium oxide (63, 64), and nickel oxide (65). This article will review four types of information that can be obtained from Raman characterization of supported metal oxides: identification of different metal oxide phases, structural transformations of metal oxide phases, location of the supported oxide on the oxide substrate, and the structure of the supported metal oxide phase. The examples used to demonstrate these points have been taken from the authors' Raman studies of the past few years.

RAMAN THEORY AND MOLECULAR STRUCTURE

Observations of the Raman effect were first reported in 1928 by Raman and Krishnan in the course of work carried out on the light-scattering of molecules (66). Scattered light can be thought of as comprising an elastic component — generally referred to as the Rayleigh scattering — and an inelastic component. Raman scattering may be regarded as an inelastic collision of an incident photon with a molecule either in its ground energy state or in an excited energy state. In contrast with fluorescence and phosphorescence, the Raman effect does not require the incident light to be coincident with an absorption band because the photon is never entirely absorbed. The photon merely perturbs the molecule, thereby inducing a vibrational or rotational transition. Consequently, in principle, any wavelength of light can be used to study the Raman effect.

The Raman effect is concerned with the polarizability of the molecule and the dipole moment induced or distorted by the electric field

of the incident light (67). Given the relatively large masses of the atomic nuclei and incident light of high enough frequency, the exchange of energy between the incident photon and the rotational or vibrational motions of the molecule results almost entirely from the polarizability of the electrons (68). The selection rule for a vibrational Raman spectrum depends on whether the polarizability changes when the molecule vibrates. If this occurs, then the vibration is Raman active. For a linear polyatomic molecule composed of N nuclei, the molecule may vibrate $3N-5$ ways, whereas a nonlinear polyatomic molecule may vibrate $3N-6$ ways. These two species possess a maximum of $3N-5$ and $3N-6$ fundamental vibrational modes, respectively.

The vibrational selection rules of the Raman effect are based entirely on symmetry considerations. Thus, if the structure for a given molecule were known, a thorough application of vibrational analysis — based on the pertinent symmetry elements of the free molecule — could be used to determine the number of permitted fundamental frequencies as well as the entire Raman spectrum (69). Generally, the vibrations of a particular common group of atoms or functional group are relatively independent of the rest of the molecule and vibrate within a specific range of frequencies. This group frequency approach allows the qualitative assignment of molecular species by carefully fingerprinting experimental spectra against those from compounds of known structure. For example, if two separate structures were proposed for an unknown compound, the vibrational analysis would predict two different Raman spectra. A comparison with the actual Raman spectrum would tend to support one of the proposed structures and not the other.

The discrimination between alternate models of differing molecular geometries that might be proposed for a given molecular species becomes a viable task when vibrational modes are assessed (70). For an undistorted, tetrahedral molecule of type MO_4 (T_d symmetry group), there are four fundamental vibrational modes [$\nu_1(A_1) + \nu_2(E) + \nu_3(F_2) + \nu_4(F_2)$], and all are Raman active. As the symmetry is lowered (that is, C_{3v}, C_{2v}, and so on), still more of the nine possible fundamentals ($3N-6$) become Raman active. For an undistorted octahedral molecule of type MO_6 (O_h symmetry group), there are three Raman active vibrational modes [$\nu_1(A_{1g}) + \nu_2(E_g) + \nu_3(F_{2g})$], and as distortions occur and the high degree of symmetry is lost (with, for example, D_{4h}, D_{2h}, and D_{3d}), a progressively greater number of the 15 possible fundamental modes become Raman active. The Raman spectrum may be further complicated by other effects (including combination bands, overtones, and lattice modes) that are not regarded as fundamental mode splitting because of a lowering of symmetry, which may result in a greater number of observed bands than would normally be expected (71–75). Application of the above information to Raman studies of supported metal oxides has provided very detailed molecular information about the supported metal oxide phases. Several examples will be discussed in this article to demonstrate the wealth of fundamental information provided by laser Raman spectroscopy of supported metal oxides.

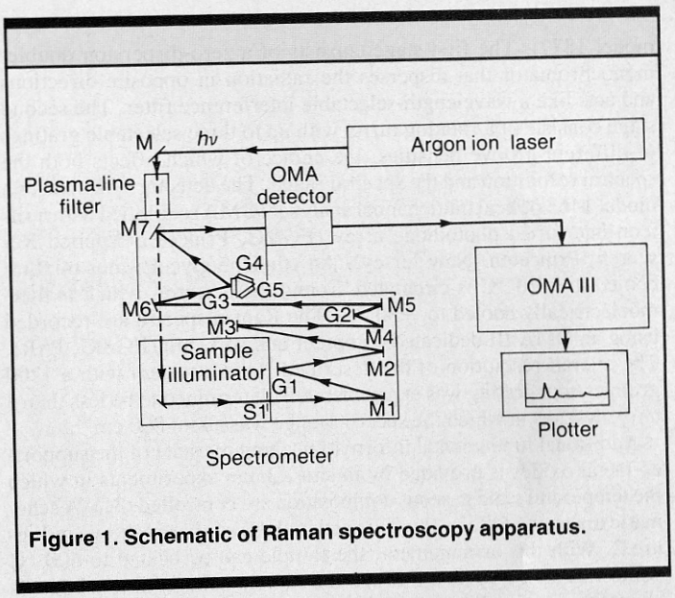

Figure 1. Schematic of Raman spectroscopy apparatus.

EXPERIMENTAL

A schematic diagram of the experimental setup used in the authors' laboratory is presented in Figure 1. A model 2020-05 Ar^+ laser (Spectra-Physics, Mountain View, California) is used to deliver the incident radiation, typically 514.5 nm, and the plasma lines are removed with a model 1460 tunable excitation filter (Spex Industries, Edison, New Jersey). The 1–100 mW incident radiation excites the sample within the sample illuminator (Spex, model 1459), and the scattered light is then directed into a Triplemate spectrometer (Spex,

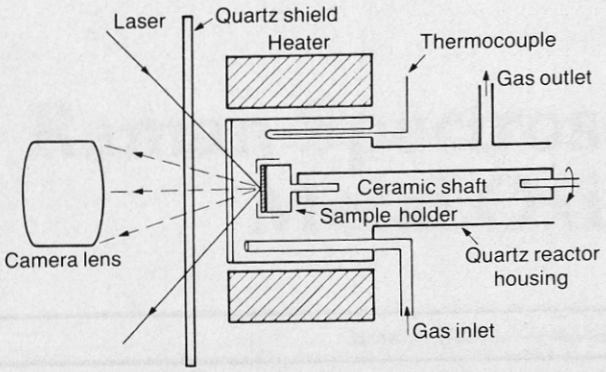

Figure 2. Schematic of in situ cell arrangement.

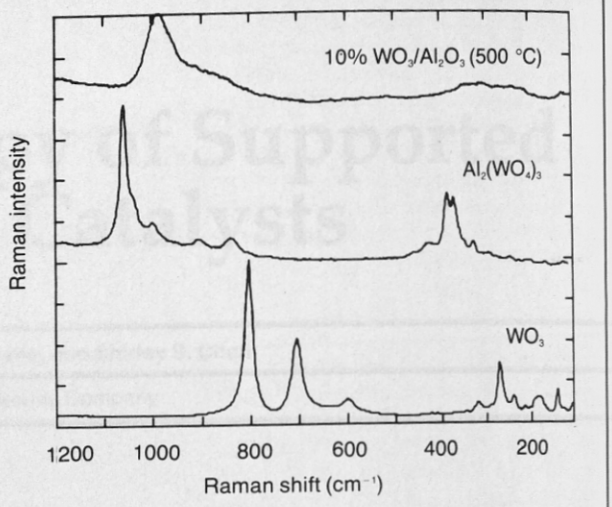

Figure 3. Raman spectra of crystalline WO_3, crystalline $Al_2(WO_4)_3$, and 10% WO_3/Al_2O_3.

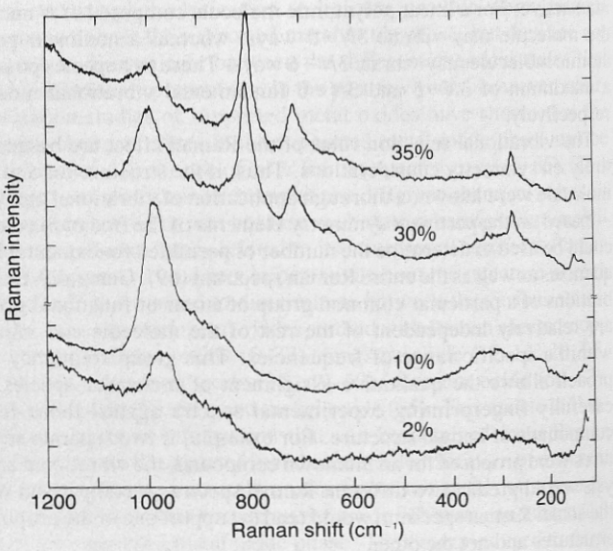

Figure 4. Raman spectra of WO_3/Al_2O_3 as a function of tungsten oxide content.

model 1877). The first stage consists of a zero-dispersion double-monochromator that disperses the radiation in opposite directions and acts like a wavelength-selectable interference filter. The second stage consists of a rotating turret with up to three selectable gratings of different groove densities, the choice of which affects both the spectral resolution and the spectral range. The detector system uses a model 1463 optical mutichannel analyzer (OMA) equipped with a silicon-intensified photodiode array (EG&G, Princeton Applied Research, Princeton, New Jersey). An ethylene glyçol/water mixture cooled to −20 °C is circulated around the detector, which is thermoelectrically cooled to −30 °C. The Raman spectra are recorded using an OMA III dedicated computer and software (EG&G, PAR). The overall resolution of the described Raman system with a 1200 grooves/mm grating was experimentally determined to be less than 3 cm^{-1} in scans in which the spectral range was about 800 cm^{-1}.

Additional fundamental information about the state of the supported metal oxides is provided by in situ Raman experiments in which the temperature and gaseous composition are controlled (31). A schematic diagram of the in situ cell used in these studies is shown in Figure 2. With this arrangement, the sample can be heated to 600 °C while various gases flow through the sample cell. Additional details about the in situ cell have been described elsewhere (76).

SUPPORTED METAL OXIDES AS SURFACE OXIDES

The Raman spectra of crystalline WO_3, crystalline $Al_2(WO_4)_3$, and 10% tungsten oxide dispersed on an alumina support (10% WO_3/Al_2O_3) are presented in Figure 3. Crystalline WO_3 possesses numerous Raman active vibrational modes with the major Raman bands at 808, 711, and 273 cm^{-1} (44). Crystalline $Al_2(WO_4)_3$, formed by the solid-state reaction between tungsten oxide and alumina at elevated temperatures, exhibits strong Raman bands at 1057, 386, and 371 cm^{-1}. The 10% WO_3/Al_2O_3 sample containing the supported tungsten oxide phase does not exhibit the strong Raman bands characteristic of crystalline WO_3 or of crystalline $Al_2(WO_4)_3$, but has weak and broad bands at ~986, ~870, and ~300 cm^{-1}. The γ-Al_2O_3 support does not exhibit any Raman active modes. The relative Raman cross-sections of these tungsten oxide phases are also very different. The crystalline WO_3 band at 808 cm^{-1} is approximately 160 times stronger than the supported tungsten oxide band at ~986 cm^{-1} per unit of tungsten oxide, and the crystalline $Al_2(WO_4)_3$ Raman band at 1057 cm^{-1} is approximately five times stronger than the supported tungsten oxide band at ~986 cm^{-1} per unit of tungsten oxide. The Raman vibrational spectra reveal that the state of the supported tungsten oxide on alumina is very different from that found in crystalline WO_3 and $Al_2(WO_4)_3$. The different state of the supported tungsten oxide on alumina relative to crystalline WO_3 and $Al_2(WO_4)_3$ is also reflected in the different chemical properties — such as reducibility — of these metal oxides (48). Similar results have also been obtained with other supported metal oxides: nickel oxide (65), rhenium oxide (60–62), chromium oxide (63,64), molybdenum oxide (5–37), tungsten oxide (12–14,20,25,31,38–48), and vanadium oxide (31,49–59).

The influence of the tungsten oxide content upon the laser Raman spectra of WO_3/Al_2O_3 samples is shown in Figure 4. The major Raman band for the supported tungsten oxide phase occurs at ~971 cm^{-1} for 2% WO_3/Al_2O_3, ~986 cm^{-1} for 10% WO_3/Al_2O_3, and

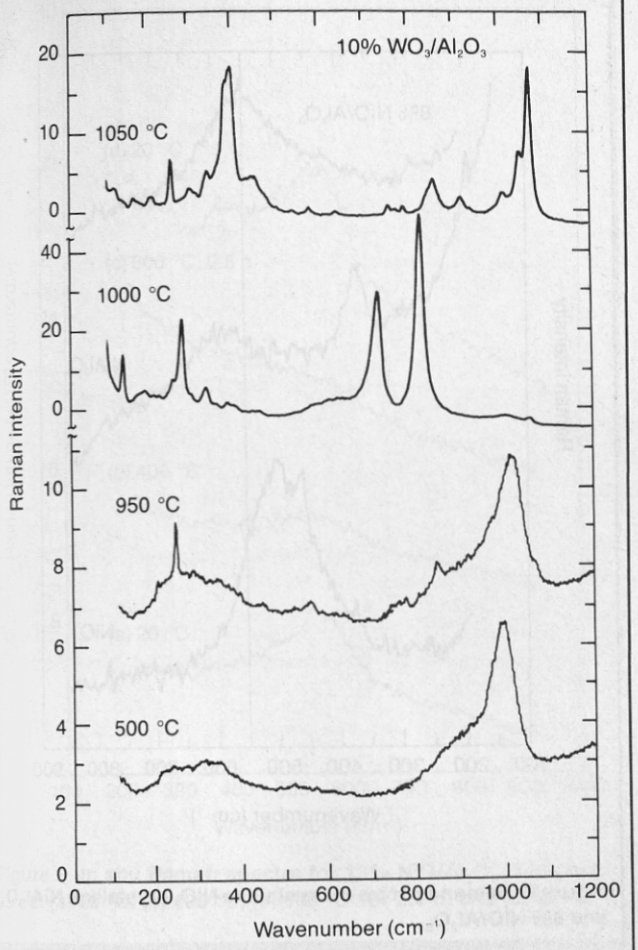

Figure 5. Raman spectra of 10% WO_3/Al_2O_3 as a function of calcination temperature.

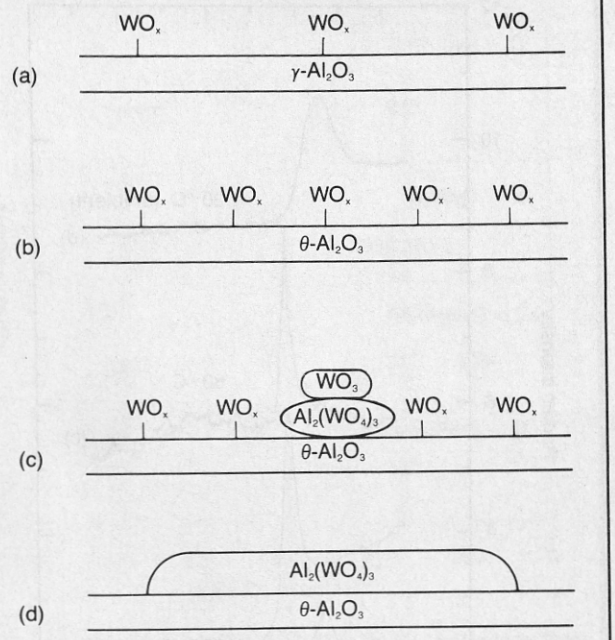

Figure 6. Structural transformations of 10% WO_3/Al_2O_3 system with calcination temperature. Structure after heating to: (a) 500 °C, (b) 950 °C, (c) 1000 °C, and (d) 1050 °C.

~1001 cm^{-1} for 30% WO_3/Al_2O_3. The laser Raman spectrum of the 30% WO_3/Al_2O_3 sample also exhibits Raman bands at 808, 711, and 273 cm^{-1}, which are characteristic of crystalline WO_3. The crystalline WO_3 Raman bands further intensify with increasing tungsten oxide content above 30% WO_3/Al_2O_3 (see Figure 4 for 35% WO_3/Al_2O_3). The Raman bands of the crystalline WO_3 phase, unlike the Raman bands of the supported tungsten oxide phase, are fixed in position and do not shift with crystalline WO_3 content. The shift in the Raman band at lower tungsten oxide content is from interactions in the supported tungsten oxide two-dimensional overlayer with increasing tungsten oxide coverage (47). The WO_3/Al_2O_3 Raman spectra in Figure 4 also reveal that the alumina support possessing ~180 m^2/g can accommodate ~30% WO_3 as a surface tungsten oxide phase (one monolayer of surface tungsten oxide); tungsten oxide in excess of this amount is present as crystalline WO_3.

SOLID-STATE CHEMISTRY OF SUPPORTED METAL OXIDES

The ability to discriminate between the different chemical states of tungsten oxide (crystalline WO_3, crystalline $Al_2(WO_4)_3$, and surface tungsten oxide) with Raman spectroscopy provides a convenient probe to monitor the structural transformations that occur in the WO_3/Al_2O_3 system with increasing temperature. The transformations that occur for 10% WO_3/Al_2O_3 as the calcination temperature is increased are shown in the Raman spectra of Figure 5. The 10% WO_3/Al_2O_3 sample treated at 500 °C exhibits only the Raman bands of the surface tungsten oxide. Additional Raman bands, however, are present at 253, 559, 743, and ~840 cm^{-1} after heating to 950 °C because of the phase transformation of γ-Al_2O_3 (Raman inactive) to θ-Al_2O_3 (major peaks at 253, 559, 743, and ~840 cm^{-1}). Furthermore, the major Raman band of the surface tungsten oxide shifts from ~986 to ~1001 cm^{-1} during this thermal treatment and reflects the increase in surface density of the tungsten oxide on the alumina support surface as a result of the significant decrease in surface area (from ~180 to ~65 m^2/g) of the alumina support (49). The surface tungsten oxide Raman band at ~1001 cm^{-1} suggests that a close-packed tungsten oxide monolayer on the alumina surface is formed during the 950 °C thermal treatment because this band position corresponds to that found for a monolayer of surface tungsten oxide on alumina (Figure 4). These structural transformations are depicted in Figures 6a and 6b.

The formation of the close-packed tungsten oxide monolayer does not preclude the alumina support from additional loss in surface area at even higher temperatures. Further heating of the 10% WO_3/Al_2O_3 sample to 1000 °C results in additional loss in surface area of the alumina support, and a portion of the surface tungsten oxide is forced to leave the monolayer to form crystalline WO_3 (major Raman bands at 808, 711, and 273 cm^{-1}) and crystalline $Al_2(WO_4)_3$ (major Raman bands at 1057, 386, and 371 cm^{-1}). The spectrum of 10% WO_3/Al_2O_3 heated to 1000 °C is dominated by the Raman bands of crystalline WO_3 because of the extremely high Raman cross-section of this phase relative to crystalline $Al_2(WO_4)_3$, surface tungsten oxide, and θ-Al_2O_3. All four phases, however, are present in the 10% WO_3/Al_2O_3 sample calcined at 1000 °C (44). After additional heating at 1050 °C, all the tungsten oxide phases in the 10% WO_3/Al_2O_3 convert to $Al_2(WO_4)_3$ — the only thermally stable tungsten oxide compound for the W-Al-O system. At these elevated temperatures, the crystal-

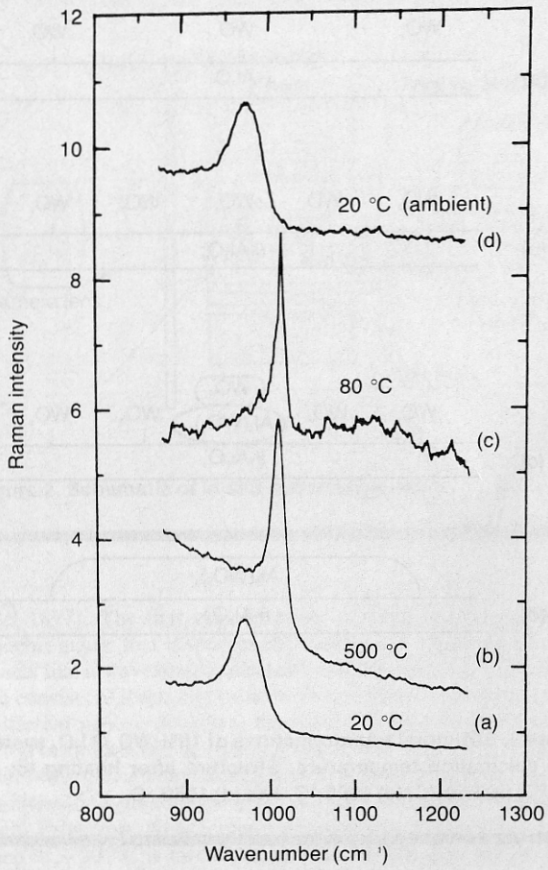

Figure 7. In situ laser Raman spectra for 7% WO_3/TiO_2. Sample at temperatures of: (a) 20 °C, (b) 500 °C, (c) 80 °C, and (d) 20 °C, ambient environment.

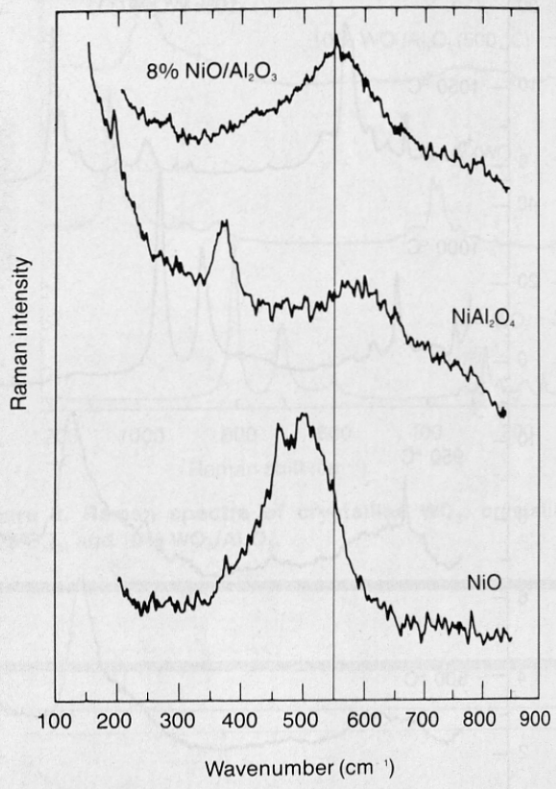

Figure 8. Raman spectra of crystalline NiO, crystalline $NiAl_2O_4$, and 8% NiO/Al_2O_3.

line WO_3 readily reacts with the alumina support to form crystalline $Al_2(WO_4)_3$. A series of detailed studies revealed that crystalline WO_3 must be present in the WO_3/Al_2O_3 sample for $Al_2(WO_4)_3$ formation to occur (45,47, 48). These changes are schematically presented in Figures 6c and 6d. The laser Raman studies reveal that the important parameter controlling the tungsten oxide phases in the WO_3/Al_2O_3 system is the surface density of the surface tungsten oxide on the alumina support.

IN SITU RAMAN SPECTROSCOPY OF SURFACE METAL OXIDES

Another advantage of the Raman technique is that experiments can be performed in situ, under conditions in which the sample environment (temperature and gas composition) can be controlled. Such experiments provide additional information about the surface metal oxide as shown in Figure 7 for 7% tungsten oxide dispersed on a titania support. The Raman spectrum of the 7% WO_3/TiO_2 sample held at room temperature (Figure 7a) exhibits a broad band at ~970 cm^{-1} that is characteristic of surface tungsten oxide (Figure 3). Heating the 7% WO_3/TiO_2 sample to 500 °C in a flowing dry-air environment results in a simultaneous sharpening and shift of the surface tungsten oxide Raman band to ~1011 cm^{-1} (Figure 7b). Additional characterization studies revealed that this thermal treatment removes moisture originally present on the sample surface from prior exposure to the ambient environment (31). Cooling the 7% WO_3/TiO_2 sample to 80 °C, as shown in Figure 7c, causes a slight sharpening of the surface tungsten oxide Raman band because of the removal of thermally induced band broadening, and the moisture-free environment maintains the Raman band at ~1011 cm^{-1}. The original broad surface tungsten oxide Raman band at ~970 cm^{-1} is only restored after the sample is exposed to moisture (Figure 7d); this spectrum resulted after exposing the 7% WO_3/TiO_2 sample to the ambient environment. This in situ experiment reveals that water molecules coordinate to the surface tungsten oxide and affect its state. The presence of the coordinated water molecules appears to increase the disorder in the two-dimensional surface oxide layer as reflected by the broadening of the surface tungsten oxide laser Raman band in the presence of moisture. The ability to adsorb and desorb water molecules from the surface tungsten oxide further reveals that the surface tungsten oxide must be *adsorbed* on the titania support surface as schematically depicted in Figure 6 for surface tungsten oxide on alumina. Similar in situ Raman behavior was also observed for other metal oxides (rhenium oxide, chromium oxide, molybdenum oxide, tungsten oxide, and vanadium oxide) on alumina and titania supports (31,33,46,61–63), demonstrating that these metal oxides are adsorbed on the oxide supports.

The Raman spectra of crystalline NiO, crystalline $NiAl_2O_4$, and 8% nickel oxide dispersed on an alumina support are presented in Figure 8. Crystalline NiO is composed of a distorted cubic NaCl structure, in which each Ni ion is coordinated by a regular octahedron of oxygen ions (77). Raman bands are observed at ~460 and ~500 cm^{-1} (65) arising from first-order defect-induced phonon scattering (78,79). Crystalline $NiAl_2O_4$, formed by the solid-state reaction between NiO and Al_2O_3 at elevated temperatures, exhibits major

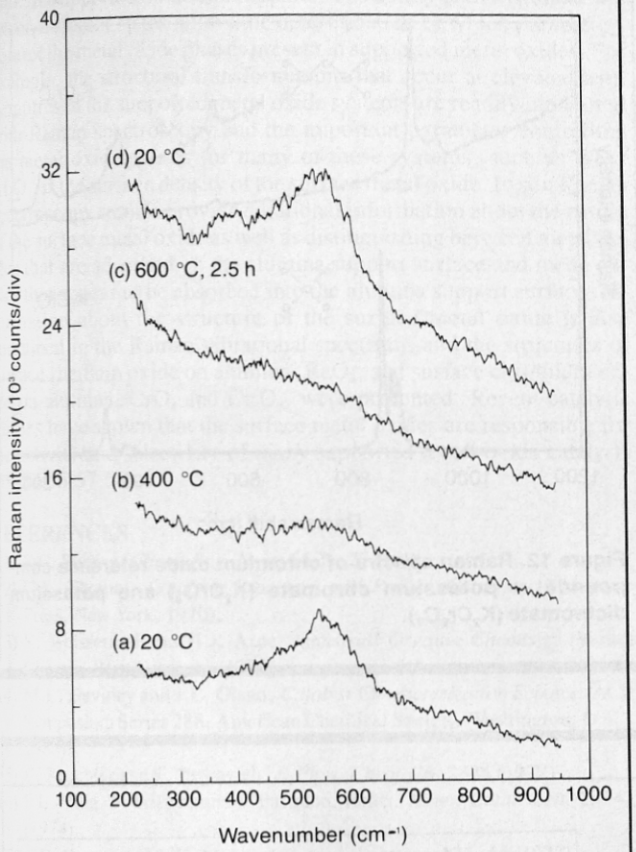

Figure 9. In situ Raman spectra for 13% NiO/Al_2O_3. Temperatures: (a) 20 °C, (b) 400 °C, (c) 600 °C for 2.5 h, and (d) 20 °C.

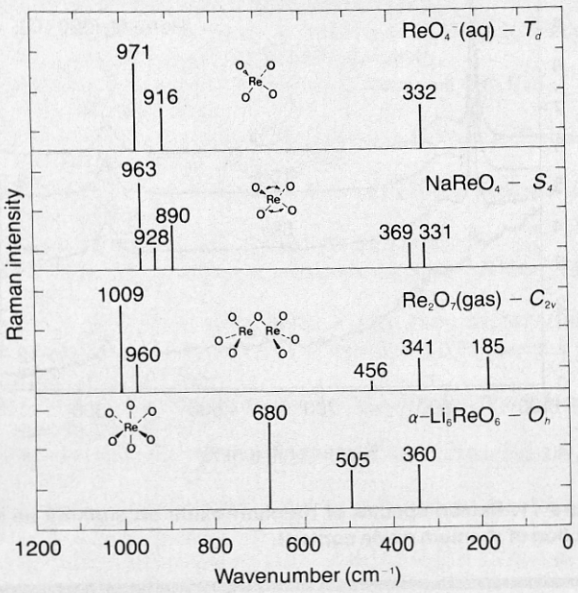

Figure 10. Raman spectra of rhenium oxide reference compounds.

Raman bands at ~600 and ~375 cm^{-1} (65). Crystalline $NiAl_2O_4$ possesses a spinel structure with Ni in octahedral and tetrahedral environments (77). The 8% NiO/Al_2O_3 sample containing the supported nickel oxide phase does not exhibit the Raman bands of crystalline NiO and $NiAl_2O_4$, but has a very broad band at ~550 cm^{-1}. The Raman vibrational spectra demonstrate, as discussed earlier for the supported tungsten oxide systems, that the state of the supported nickel oxide on alumina is very different from that found in crystalline NiO and $NiAl_2O_4$. The characteristics of the supported nickel oxide Raman vibrational spectrum, however, are very different from those earlier presented for the supported tungsten oxide phase. The supported nickel oxide on alumina possesses a Raman band at ~550 cm^{-1} that is two orders of magnitude weaker than the major Raman band at ~900–1000 cm^{-1} for the supported tungsten oxide on alumina. The different positions of the Raman bands for the supported nickel oxide and tungsten oxide reflect the types of oxygen associated with these metal oxides (74). The supported tungsten oxide Raman band at ~900–1000 cm^{-1} indicates that W=O bonds are present in the surface tungsten oxide on alumina. The supported nickel oxide Raman band at ~550 cm^{-1} indicates that only Ni-O bonds are present in the surface nickel oxide on alumina. The response of the supported nickel oxide on alumina to an in situ experiment is also very different from that presented earlier for the supported tungsten oxide, as shown in Figure 9 (65). The Raman band of the supported nickel oxide on alumina is not affected by the removal of the moisture present on the sample surface (compare Figures 9a and 9d) and suggests that water molecules do not coordinate to the supported nickel oxide. The pronounced thermal broadening of the supported nickel oxide Raman band at elevated temperatures (Figures 9b and 9c) suggests that the nickel oxide vibrational modes may be intimately coupled to the vibrations of the alumina support (79). The water insensitivity of the supported nickel oxide Raman band and its pronounced thermal broadening at elevated temperatures are consistent with the incorporation of the nickel oxide into the defects of the γ-Al_2O_3 surface (formation of a surface spinel). The ease with which nickel oxide diffuses into the alumina support is well known (80). Formation of a surface nickel oxide–alumina spinel would account for the inability of the water molecules to coordinate to the nickel oxide species and explain the intimate vibrational coupling of the nickel oxide and explain the alumina support. This hypothesis suggests that the nickel oxide is not adsorbed on the alumina support as is surface tungsten oxide, but that the surface nickel oxide is *absorbed* into the surface of the alumina support. Thus, in situ laser Raman spectroscopy studies are capable of distinguishing between metal oxides that are adsorbed on the alumina support surface and metal oxides that appear to be absorbed into the alumina support surface as a surface spinel.

THE STRUCTURES OF SURFACE METAL OXIDES

The Raman vibrational spectrum also contains detailed information about the structure of metal oxides because the vibrational selection rules are determined by the symmetry of the coordinated compound (70). The laser Raman spectra of several rhenium oxide reference compounds are presented as stick diagrams in Figure 10. In aqueous solution $[ReO_4]^-$ assumes regular tetrahedral symmetry, T_d, and exhibits Raman bands at 971 cm^{-1} (ν_1 symmetric stretch of the ReO_4 group), 916 cm^{-1} (ν_3 antisymmetric stretch of the ReO_4 group), and 332 cm^{-1} (ν_2 symmetric and ν_4 antisymmetric bending modes of the ReO_4 group) (81). Tetrahedrally coordinated compounds can give rise to four Raman active modes, but aqueous $[ReO_4]^-$ exhibits only three Raman modes because the bending modes are degenerate and unresolvable (82). In solid perrhenates (NH_4ReO_4, $KReO_4$, and $NaReO_4$) the $[ReO_4]^-$ ions assume distorted tetrahedral structures consistent with S_4 site symmetry (83). For such slightly distorted tet-

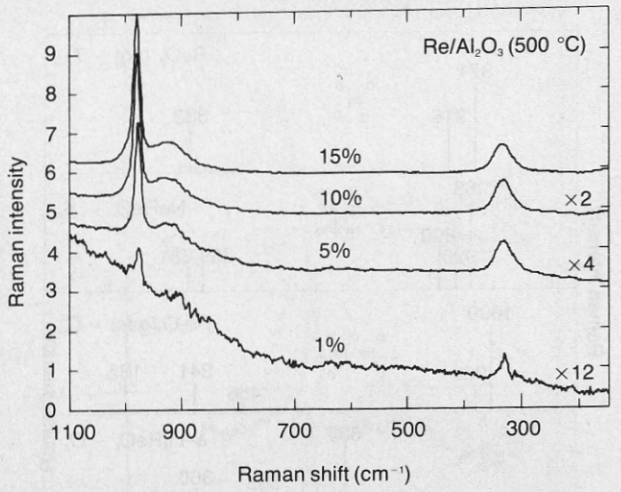

Figure 11. Raman spectra of rhenium oxide on alumina as a function of rhenium oxide content.

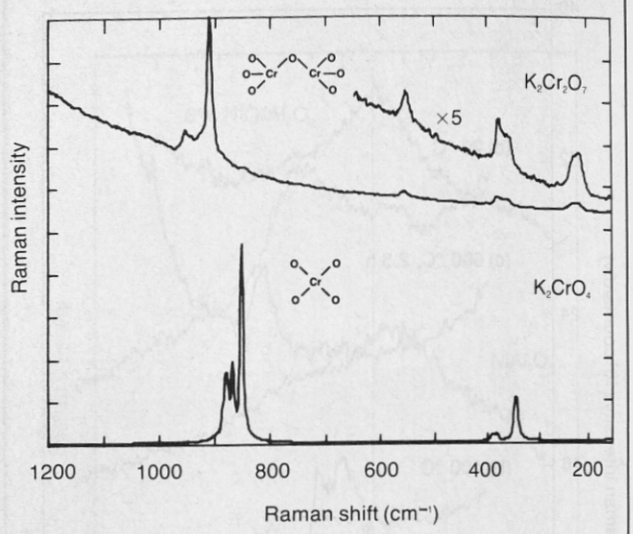

Figure 12. Raman spectra of chromium oxide reference compounds — potassium chromate (K_2CrO_4) and potassium dichromate ($K_2Cr_2O_7$).

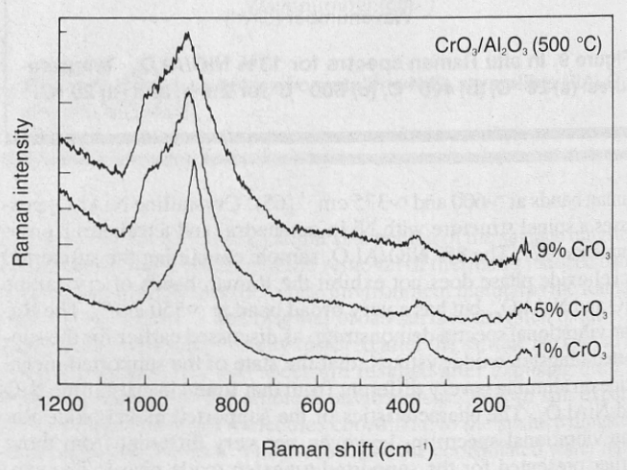

Figure 13. Raman spectra of CrO_3/Al_2O_3 as a function of chromium oxide content.

rahedrally coordinated compounds, the antisymmetric modes, ν_3 and ν_4, and the symmetric bending mode, ν_2, are split into doublets (83). Gaseous Re_2O_7 consists of two tetrahedral ReO_3 groups that contain one bridging oxygen between them and exhibit Raman bands at 1009 cm^{-1} (symmetric stretch), 960 cm^{-1} (antisymmetric stretch), 341 cm^{-1} (symmetric and antisymmetric bending modes), 456 cm^{-1} (symmetric stretch of the bridging Re-O-Re group), and 185 cm^{-1} (bending of the bridging Re-O-Re) (85). The Raman spectrum of compounds possessing rhenium oxide in octahedral coordination exhibits a very different vibrational spectrum. For regular octahedral symmetry, only three modes are Raman active (67). The compound α-Li_6ReO_6 possesses regular octahedral symmetry and has Raman bands at 680 cm^{-1} (symmetric stretch), 505 cm^{-1} (antisymmetric stretch), and 360 cm^{-1} (bending mode) (84). The positions of the Raman bands for regular octahedral symmetry and relative peak positions are very different from those present in the Raman spectra of tetrahedral compounds and reflect the different types of rhenium-oxygen bonds present in each case (85). These differences in peak positions are related to the presence of Re=O bonds in the tetrahedral compounds and Re-O bonds in the regular octahedral compound. Comparison of the spectrum of rhenium oxide on alumina (Figure 11) with the spectra of the reference compounds (Figure 10) permits the determination of the coordination of the supported rhenium oxide on alumina. The Raman spectra of rhenium oxide on alumina possess vibrational bands at 980, 920, and 335 cm^{-1}, which are independent of rhenium oxide surface coverage. These Raman features are consistent with the presence of isolated, tetrahedrally coordinated surface rhenium oxide, ReO_4, on the alumina support.

Chromium (VI) oxide compounds, specifically the mono- and dichromates, consist of tetrahedrally coordinated chromium atoms in both the crystalline phase (86–88) and in aqueous solution (89). The Raman spectra of the chromates are quite similar to those found for the tetrahedrally coordinated rhenium oxide compounds, with the exception of the reversed order of symmetric and antisymmetric stretching band frequencies ($\nu_1 > \nu_3$ for rhenium oxide and $\nu_3 > \nu_1$ for chromium oxide) (70). The Raman spectra for K_2CrO_4 and $K_2Cr_2O_7$ are shown in Figure 12, which compares the monochromate with the dichromate species, in which a Cr-O-Cr linkage is present. In comparison to the monochromate, the dichromate exhibits higher symmetric and antisymmetric stretching frequencies (853 → 911 cm^{-1}, 880 → 961 cm^{-1}, and 868 → 945 cm^{-1}) as well as a Cr-O-Cr symmetric stretch at 565 cm^{-1} and Cr-O-Cr bending mode at 228 cm^{-1}. The Raman spectra for chromium oxide on alumina are presented in Figure 13. Note that the CrO_3/Al_2O_3 spectra exhibit Raman bands consistent with monochromate as well as a small band at ~225 cm^{-1} from the bending mode of the Cr-O-Cr group. Thus, the chromium oxide Raman spectra reveal that the surface chromium oxide is present as an isolated, tetrahedrally coordinated surface chromium oxide, CrO_4, in addition to as a dichromate surface chromium oxide species, Cr_2O_7.

CONCLUSION

This article reviewed the types of fundamental information that are currently obtainable from the Raman characterization of supported

metal oxide catalysts. The Raman vibrational spectra reveal that the states of the supported metal oxides are very different from their bulk, unsupported oxide counterparts. The ability to discriminate between different states allows the determination of which parameters control the metal oxide phases present in supported metal oxides. For example, the structural transformations that occur at elevated temperatures in the supported metal oxide systems are readily monitored with Raman spectroscopy and the important parameter controlling the metal oxide phases for many of these systems, such as WO_3/Al_2O_3, is the surface density of the surface metal oxide. In situ Raman spectroscopy studies provide additional information about the nature of the surface metal oxide as well as distinguishing between metal oxides that are adsorbed on the alumina support surface and metal oxides that appear to be absorbed into the alumina support surface. Information about the structure of the surface metal oxide is also contained in the Raman vibrational spectrum, and the structures of surface rhenium oxide on alumina, ReO_4, and surface chromium oxide on alumina, CrO_4 and Cr_2O_7, were presented. Recent catalytic studies have shown that the surface metal oxides are responsible for the activity and selectivity of many supported metal oxide catalysts (35,53,55,57,58).

REFERENCES

(1) S.C. Stinson, *Chem. Eng. News* **64**(7), 27 (1986).

(2) C.L. Thomas, *Catalytic Processes and Proven Catalysts* (Academic Press, New York, 1970).

(3) K. Weissermel and H.J. Arpe, *Industrial Organic Chemistry* (Verlag Chemie, West Germany, 1970).

(4) M.L. Deviney and J.L. Gland, *Catalyst Characterization Science* (ACS Symposium Series 288, American Chemical Society, Washington, D.C., 1985).

(5) E. Beuchler and J. Turkevich, *J. Phys. Chem.* **76,** 2325 (1972).

(6) P.L. Villa, F. Trifiro, and I. Pasquon, *React. Kinet. Catal. Lett.* **1,** 341 (1974).

(7) F.R. Brown and L.E. Makovsky, *Appl. Spectrosc.* **31,** 44 (1977).

(8) F.R. Brown, L.E. Makovsky, and K.H. Rhee, *J. Catal.* **50,** 162 (1977).

(9) F.R. Brown, L.E. Makovsky, and K.H. Rhee, *J. Catal.* **50,** 385 (1977).

(10) J. Medema, C. van Stam, V.H.J. deBeer, A.J.A. Konings, and D.C. Koningsberger, *J. Catal.* **53,** 386 (1978).

(11) H. Knozinger and H. Jeziorowski, *J. Phys. Chem.* **82,** 2002 (1978).

(12) A. Iannibello, S. Marengo, F. Trifiro, and P.L. Villa, in *Preparation of Catalysts II,* B. Delmon, P. Grange, P. Jacobs, and P. Poncelet, eds. (Elsevier, Amsterdam, 1979), p. 65.

(13) R. Thomas, M.C. Mittelmeijer-Hazeleger, F.P.J.M. Kerkhof, J.A. Moulijn, J. Medema, and V.H.J. deBeer, *Proceedings of the Climax Third International Conference on Chemistry and Uses of Molybdenum,* H.F. Barry and P.C.H. Mitchell, eds. (Climax Molybdenum Company, Ann Arbor, Michigan, 1979), p. 85.

(14) R. Iannibello, S. Marengo, and P.L. Villa, ibid., p. 92.

(15) C.P. Cheng and G.L. Schrader, *J. Catal.* **60,** 276 (1979).

(16) H. Jeziorowski and H. Knozinger, *J. Phys. Chem.* **83,** 1166 (1980).

(17) H. Knozinger, H. Jeziorowski, and E. Taglauer, in *Proc. Seventh Intern. Congr. Catal.*, T. Seiyama and K. Tanabe, eds. (1980), p. 604.

(18) D.S. Zingg, L.E. Makovsky, R.E. Tischer, F.R. Brown, and D.M. Hercules, *J. Phys. Chem.* **84,** 2898 (1980).

(19) L. Wang and W.K. Hall, *J. Catal.* **66,** 251 (1980).

(20) R. Thomas, J.A. Moulijn, V.H.J. deBeer, and J. Medema, *J. Mol. Catal.* **8,** 161 (1980).

(21) P. Defresne, E. Payen, J. Grimblot, and J.P. Bonnelle, *J. Phys. Chem.* **85,** 2344 (1981).

(22) A. Lopez Agudo, F.J. Gil, J.M. Callega, and V. Fernandez, *J. Raman Spectrosc.* **11,** 454 (1981).

(23) E. Payen, M.C. Dhamelincourt, P. Dhamelincourt, J. Grimblot, and J.P. Bonnelle, *Appl. Spectrosc.* **36,** 30 (1982).

(24) W.K. Hall, *Proceedings of the Climax Fourth International Conference on Chemistry and Uses of Molybdenum,* H.F. Barry and P.C.H. Mitchell, eds. (Climax Molybdenum Company, Ann Arbor, Michigan, 1982), p. 224.

(25) A.I. Iannibelli, S. Marengo, G. Morelli, and P. Titarelli, ibid., p. 256.

(26) J. Grimblot, E. Payen, and J.P. Bonnelle, ibid., p. 261.

(27) S. Kasztelan, J. Grimblot, J.P. Bonnelle, E. Payen, H. Toulhoat, and Y. Jacquin, *Appl. Catal.* **7,** 91 (1983).

(28) G.L. Schrader and C.P. Cheng, *J. Catal.* **80,** 369 (1983).

(29) L. Wang and W.K. Hall, *J. Catal.* **83,** 242 (1983).

(30) M. Kantschewa, F. Delannay, H. Jeziorowski, E. Delgado, S. Eder, G. Ertl, and H. Knozinger, *J. Catal.* **87,** 482 (1984).

(31) S.S. Chan, I.E. Wachs, L.L. Murrell, L. Wang, and W.K. Hall, *J. Phys. Chem.* **88,** 5831 (1984).

(32) J.M. Stencel, L.E. Makovsky, T.A. Sarkus, J. DeVries, R. Thomas, and J.A. Moulijn, *J. Catal.* **90,** 314 (1984).

(33) J.M. Stencel, L.E. Makovsky, J.R. Diehl, and T.A. Sarkus, *J. Catal.* **95,** 414 (1985).

(34) K.Y.S. Ng and E. Gulari, *J. Catal.* **92,** 340 (1985).

(35) Y.C. Liu, G.L. Griffin, S.S. Chan, and I.E. Wachs, *J. Catal.* **94,** 108 (1985).

(36) K.Y.S. Ng, X. Zhou, and E. Gulari, *J. Phys. Chem.* **89,** 2477 (1985).

(37) J.P. Baltrus, L.E. Makovsky, J.M. Stencel, and D.M. Hercules, *Anal. Chem.* **57,** 2500 (1985).

(38) R. Thomas, J.A. Moulijn, and F.P.J.M. Kerkhof, *Rec. Trav. Chim. Pay-Bas.* **96,** 134 (1977).

(39) A. Iannibello, P.L. Villa, and S. Marengo, *Gazz. Chim. Ital.* **109,** 5121 (1979).

(40) R. Thomas, F.P.J.M. Kerkhof, J.A. Moulijn, J. Medema, and V.H.J. deBeer, *J. Catal.* **61,** 559 (1980).

(41) R. Thomas, V.H.J. deBeer, and J.A. Moulijn, *Bull. Soc. Chim. Belg.* **90,** 1349 (1981).

(42) L. Salvati, Jr., L.E. Makovsky, J.M. Stencel, F.R. Brown, and D.M. Hercules, *J. Phys. Chem.* **85,** 3799 (1981).

(43) P. Titarelli, A. Iannibello, and P.L. Villa, *J. Solid State Chem.* **37,** 95 (1981).

(44) S.S. Chan, I.E. Wachs, and L.L. Murrell, *J. Catal.* **90,** 150 (1984).

(45) S.S. Chan, I.E. Wachs, L.L. Murrell, and N.C. Dispenziere, Jr., in *Catalysis on the Energy Scene,* S. Kaliaguine and A. Mahay, eds. (Elsevier, Amsterdam, 1984), p. 259.

(46) J.M. Stencel, L.E. Makovsky, J.R. Diehl, and T.A. Sarkus, *J. Raman Spectrosc.* **15,** 282 (1984).

(47) S.S. Chan, I.E. Wachs, L.L. Murrell, and N.C. Dispenziere, Jr., *J. Catal.* **92,** 1 (1985).

(48) S. Soled, L.L. Murrell, I.E. Wachs, G.B. McVicker, L.G. Sherman, S.S. Chan, N.C. Dispenziere, and R.T.K. Baker, in *Solid State Chemistry in Catalysis,* R.K. Grasselli and J.F. Brazdil, eds. (ACS Symposium Series 279, American Chemical Society, Washington, D.C., 1985), p. 165.

(49) F. Roozeboom, J. Medema, and P.J. Gellings, *Z. Phys. Chem.* (Frankfurt am Main) **111,** 215 (1978).

(50) F. Roozeboom, M.C. Mittelmeijer-Hazeleger, J.A. Moulijn, J. Medema, V.H.J. deBeer, and P.J. Gellings, *J. Phys. Chem.* **84,** 2783 (1980).

(51) A.J. Van Hengstum, J.G. Van Ommen, H. Bosch, and P.J. Gellings, *Appl. Catal.* **5,** 207 (1983).

(52) I.E. Wachs and S.S. Chan, *Appl. Surf. Sci.* **20,** 181 (1984).

(53) I.E. Wachs, S.S. Chan, C.C. Chersich, and R.Y. Saleh, in *Catalysis on the Energy Scene,* S. Kaliaguine and A. Mahay, eds. (Elsevier, Amsterdam, 1984), p. 275.

(54) I.E. Wachs, S.S. Chan, and C.C. Chersich, in *Reactivity of Solids,* P. Barret and L.C. Dufour, eds. (Elsevier, Amsterdam, 1985), p. 1047.

(55) I.E. Wach, R.Y. Saleh, S.S. Chan, and C.C. Chersich, *Appl. Catal.* **15,** 339 (1985).

(56) I.E. Wachs, S.S. Chan, and R.Y. Saleh, *J. Catal.* **91,** 366 (1985).

(57) I.E. Wachs, R.Y. Saleh, S.S. Chan, and C.C. Chersich, *CHEMTECH* **15,** 756 (1985).

(58) R.Y. Saleh, I.E. Wachs, S.S. Chan, and C.C. Chersich, *J. Catal.* **98,** 102 (1986).

(59) R.Y. Saleh, I.E. Wachs, S.S. Chan, and C.C. Chersich, *Preprints, Div. Petrol. Chem.*, ACS, **31,** 272 (1986).

(60) F.P.J.M. Kerkhof, J.A. Moulijn, and R. Thomas, *J. Catal.* **56,** 279 (1979).

(61) L. Wang and W.K. Hall, *J. Catal.* **82,** 177 (1983).

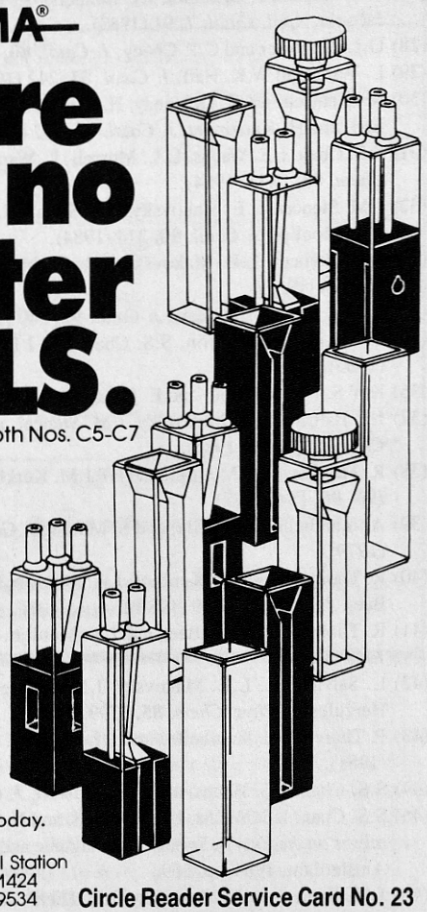

(62) F.D. Hardcastle and I.E. Wachs, *J. Catal.*, manuscript submitted.
(63) L. Wang, thesis, University of Wisconsin–Milwaukee (1982).
(64) F.D. Hardcastle and I.E. Wachs, in preparation.
(65) S.S. Chan and I.E. Wachs, *J. Catal.*, in press.
(66) C.V. Raman and K.S. Krishnan, *Nature* **121,** 501 (1928).
(67) E.B. Wilson, J.C. Decius, and P.C. Cross, *Molecular Vibrations: The Theory of Infrared and Raman Vibrational Spectra* (Dover Publications, New York, 1980).
(68) G. Placzek, *Marx Handbuch der Radiologie*, vol. 6, part 2 (Akademische Verlagsgesellschaft M.B.H., Leipzig, 1934), pp. 209–374.
(69) F.A. Cotton, *Chemical Applications of Group Theory* (Wiley-Interscience, New York, 1971).
(70) K. Nakamoto, *Infrared and Raman Spectra of Inorganic and Coordination Compounds* (John Wiley & Sons, New York, 3rd Ed., 1978).
(71) G. Herzberg, *Infrared and Raman Spectra of Polyatomic Molecules: Molecular Spectra and Molecular Structure, II* (Van Nostrand Reinhold Company, New York, 1945).
(72) R.S. Halford, *J. Chem. Phys.* **14,** 8 (1946).
(73) W.G. Fateley, *Appl. Spectrosc.* **27,** 395 (1973).
(74) I.R. Beattie and T.R. Gilson, *J. Chem. Soc. (A)*, 2322 (1969).
(75) Z. Iqbal and F.J. Owens, *Vibrational Spectroscopy of Phase Transitions* (Academic Press, New York, 1984).
(76) S.S. Chan and A.T. Bell, *J. Catal.* **89,** 433 (1984).
(77) A.F. Wells, *Structural Inorganic Chemistry* (Clarendon Press, Oxford, 1984).
(78) R.E. Dietz, G.I. Parisot, and A.E. Meixner, *Phys. Rev.* **B4,** 2302 (1971).
(79) C.H. Perry, E. Anastassakis, and J. Sokoloff, *Ind. J. Pure Appl. Phys.* **9,** 930 (1971).
(80) L.E. Alzarmora, J.R.H. Ross, E.C. Kruissink, and L.L. van Reijnen, *J. Chem. Soc., Faraday Trans. 1* **77,** 665 (1981).
(81) F. Gonzelez-Vilchez and W.P. Griffith, *J. Chem. Soc., Dalton Trans.* **13,** 1416 (1972).
(82) L.A. Woodward and H.L. Roberts, *Trans. Faraday Soc.* **52,** 615 (1956).
(83) R.A. Johnson, M.T. Rogers, and G.E. Leroi, *J. Chem. Phys.* **56,** 789 (1972).
(84) J. Hauck and A. Fadini, *Z. Naturforsch* **25B,** 422 (1970).
(85) I.R. Beattie and G.A. Ozin, *J. Chem. Soc. (A)*, 2615 (1969).
(86) J.S. Stephens and D.W.J. Cruickshank, *Acta Crystallogr.* **B26,** 437 (1970).
(87) J.K. Brandon and I.D. Brown, *Can. J. Chem.* **46,** 933 (1968).
(88) H. Stammreich, D. Bassi, O. Sala, and H. Siebert, *Spectrochim. Acta* **13,** 192 (1958).
(89) G. Michel and R. Cahay, *J. Raman Spectrosc.* **17,** 79 (1986).

Israel E. Wachs, *Corporate Research Science Laboratories, Exxon Research and Engineering Company, Annandale, New Jersey 08801, received his chemical engineering degrees from the City College of the City University of New York (BE) and Stanford University (MS and PhD). He has been employed by the Corporate Research Science Laboratories since graduating from Stanford. Wachs is interested in fundamental and applied research of heterogeneous catalysis.*

Franklin D. Hardcastle *received his BS in chemistry from Montana State University and his MS in physical-analytical chemistry from the University of Utah. He was hired by Exxon Research and Engineering Company in 1985 and has been involved in the application of spectroscopic techniques, including laser Raman spectroscopy, to the fundamental and applied research of heterogeneous catalysis.*

Shirley Suiling Chan *received her BS in physics from Western Illinois University and her MS in physics and PhD in biophysics from the University of Illinois, Urbana. In both her graduate research and in postdoctoral research at the Max Planck Institute for Biophysical Chemistry, she applied laser spectroscopies to studies of protein and cell dynamics. At Exxon, Chan applied Raman spectroscopy to the studies of heterogeneous catalysts and developed an in situ system. Chan is currently a senior scientist at the Technical Center of the BOC Group (100 Mountain Avenue, Murray Hill, New Jersey 07974) and is engaged in research and development of health care instruments.*